A Conserved Sequence from Heat-Adapted Species Improves Rubisco Activase Thermostability in Wheat[1][OPEN]

Andrew P. Scafaro,[a,b,2,3] Nadine Bautsoens,[a] Bart den Boer,[a] Jeroen Van Rie,[a] and Alexander Gallé[a]

[a]BASF Agricultural Solutions, Ghent 9052, Belgium
[b]Australian Research Council Centre of Excellence in Plant Energy Biology, Research School of Biology, Australian National University, Canberra, Australian Capital Territory 2601, Australia

ORCID IDs: 0000-0003-3738-1145 (A.P.S.); 0000-0002-3886-108X (B.d.B.).

The central enzyme of photosynthesis, Rubisco, is regulated by Rubisco activase (Rca). Photosynthesis is impaired during heat stress, and this limitation is often attributed to the heat-labile nature of Rca. We characterized gene expression and protein thermostability for the three Rca isoforms present in wheat (*Triticum aestivum*), namely TaRca1-β, TaRca2-α, and TaRca2-β. Furthermore, we compared wheat Rca with one of the two Rca isoforms from rice (*Oryza sativa*; OsRca-β) and Rca from other species adapted to warm environments. The *TaRca1* gene was induced, whereas *TaRca2* was suppressed by heat stress. The TaRca2 isoforms were sensitive to heat degradation, with thermal midpoints of 35°C $\pm$ 0.3°C, the temperature at which Rubisco activation velocity by Rca was halved. By contrast, TaRca1-β was more thermotolerant, with a thermal midpoint of 42°C, matching that of rice OsRca-β. Mutations of the TaRca2-β isoform based on sequence alignment of the thermostable TaRca1-β from wheat, OsRca-β from rice, and a consensus sequence representing Rca from warm-adapted species enabled the identification of 11 amino acid substitutions that improved its thermostability by greater than 7°C without a reduction in catalytic velocity at a standard 25°C. Protein structure modeling and mutational analysis suggested that the thermostability of these mutational variants arises from monomeric and not oligomeric thermal stabilization. These results provide a mechanism for improving the heat stress tolerance of photosynthesis in wheat and potentially other species, which is a desirable outcome considering the likelihood that crops will face more frequent heat stress conditions over the coming decades.

Rubisco is the central enzyme of photosynthesis, converting inert CO_2 gas from the atmosphere into sugars. Rubisco is tightly regulated, and the active site of Rubisco is prone to inhibition, even by its phosphate sugar substrate ribulose-1,5-bisphosphate (RuBP; Parry et al., 2008). The regulation of Rubisco and removal of inhibitors from the Rubisco active site are performed by its chaperone enzyme Rubisco activase (Rca; Portis, 2003). Rca is a member of the AAA^+ family of enzymes and utilizes ATP to mechanically remove tightly bound inhibitors from the Rubisco active site (Mueller-Cajar, 2017). One of the defining characteristics of Rca is that it is a heat-labile protein and in many species dissociates, denatures, and aggregates with even moderate heat application, to a much greater extent than Rubisco (Feller et al., 1998; Salvucci et al., 2001; Salvucci and Crafts-Brandner, 2004). As such, Rca is considered one of the main causes of a decrease in photosynthetic function for plants exposed to supraoptimal temperatures (Crafts-Brandner and Salvucci, 2000; Sage et al., 2008; Busch and Sage, 2017; Perdomo et al., 2017). Improving the thermostability of Rca is therefore considered one of the most promising ways of improving photosynthesis and thus potentially the yield of crops exposed to the detrimental impacts of heat stress (Parry et al., 2011; Carmo-Silva et al., 2015).

The thermal stability of Rca is dependent on species and correlates with the climate in which a species has evolved, with temperate species having Rca that is heat labile relative to tropical species (Carmo-Silva and Salvucci, 2011; Henderson et al., 2013). Even closely related species from varying environments, such as between rice (*Oryza sativa*) and its close relative *Oryza australiensis*, endemic to hot environments in the northern regions of Australia, have divergent thermostable variants of Rca (Scafaro et al., 2016). The genetic diversity in thermostability of Rca between species is

[1]This work was supported by a Marie Skłodowska-Curie Individual Fellowship from the European Commission (706115 Heat Wheat) and by the Department of Industry, Innovation, Science, Research, and Tertiary Education, Australian Government/Australian Research Council (CE140100008) to A.P.S.

[2]Author for contact: andrew.scafaro@anu.edu.au.
[3]Senior author.
The author responsible for distribution of materials integral to the findings presented in this article in accordance with the policy described in the Instructions for Authors (www.plantphysiol.org) is: Andrew P. Scafaro (andrew.scafaro@anu.edu.au).

A.P.S., B.d.B., J.V.R., and A.G. conceived and planned experiments; A.P.S. and N.B. conducted the experiments; A.P.S. analyzed data and drafted the article with support from all other authors.

[OPEN]Articles can be viewed without a subscription.
www.plantphysiol.org/cgi/doi/10.1104/pp.19.00425

currently being explored to improve the stability of more susceptible Rca variants. For example, a recent study looked at improving rice Rca thermostability based on the more thermostable Rca from *Agave tequilana*, a Crassulacean acid metabolism desert plant (Shivhare and Mueller-Cajar, 2017).

Wheat (*Triticum aestivum*) is a temperate grass with short-term photosynthesis impairment at temperatures above 35°C (Silva-Pérez et al., 2017). However, acclimation to warmer growing conditions can increase the optimum temperature of photosynthesis in wheat (Yamasaki et al., 2002), suggesting longer-term biochemical adjustments to higher temperatures. In many species, including rice, there is a single functional Rca gene that encodes two protein isoforms based on alternative splicing of pre-mRNA into a larger α-isoform and a shorter β-isoform (To et al., 1999; Nagarajan and Gill, 2018). Similarly, for wheat, there is an α- and a β-isoform, but wheat has an additional Rca gene that encodes a second variant of the β-isoform. The latter gene is referred to as form 1 and the former alternatively spliced gene is referred to as form 2 (Carmo-Silva et al., 2015; Nagarajan and Gill, 2018). Thus, in wheat, excluding the nearly identical copies on each of the three wheat chromosome subgenomes, there are three distinct Rca gene products that can be expressed: a form 1β (TaRca1-β), form 2α (TaRca2-α), and form 2β (TaRca2-β). The relative expression and protein abundance of these three isoforms in relation to one another may be an important factor in wheat heat stress tolerance. Higher amounts of *TaRca2-α* expression under nonstressed physiological conditions have been reported to be linked to increased photosynthesis, biomass, and yield in wheat (Saeed et al., 2016). Furthermore, the protein profile of wheat Rca determined by western-blot analysis shows that there are two bands corresponding to an α- and a β-isoform and abundance of a third band in close proximity to the position of the original β-isoform when wheat is exposed to heat stress (Law and Crafts-Brandner, 2001; Ristic et al., 2009). It is unknown if the two Rca isoforms with similar molecular mass during heat stress relate to the TaRca1-β and TaRca2-β isoforms, although it is likely, as induction of the *TaRca1-β* gene in response to heat stress has been observed in certain cultivars of wheat (Kumar et al., 2016).

Here, we determined the expression profiles of the three Rca isoforms found in wheat and how heat stress affected expression. Following this, the in vitro thermostability of all three wheat Rca isoforms was assessed and a link was made between regulation during heat stress and Rca thermostability. The most abundant and heat-sensitive isoform of Rca in wheat, TaRca2-β, was mutated based on protein sequence comparisons with relatively thermostable wheat and rice isoforms, as well as through comparisons of Rca protein sequences between cold- and warm-adapted species. Characterization of the TaRca2-β mutants enabled the identification of as few as three to 11 amino acids that impart thermostability on the enzyme.

RESULTS

Differential expression of wheat Rca isoforms in response to temperature varied dramatically. When the spring wheat 'Fielder' was exposed to a 38°C day temperature over two diurnal cycles during its vegetative stage, there was a shift in Rca isoform expression from control at 22°C. While expression of the *TaRca2-α* isoform remained constant, there was a decline in expression of the *TaRca2-β* isoform with heat treatment (Fig. 1A). Furthermore, expression of *TaRca1-β*, which is encoded by a separate gene and has a relatively high sequence divergence compared with the *TaRca2* spliced

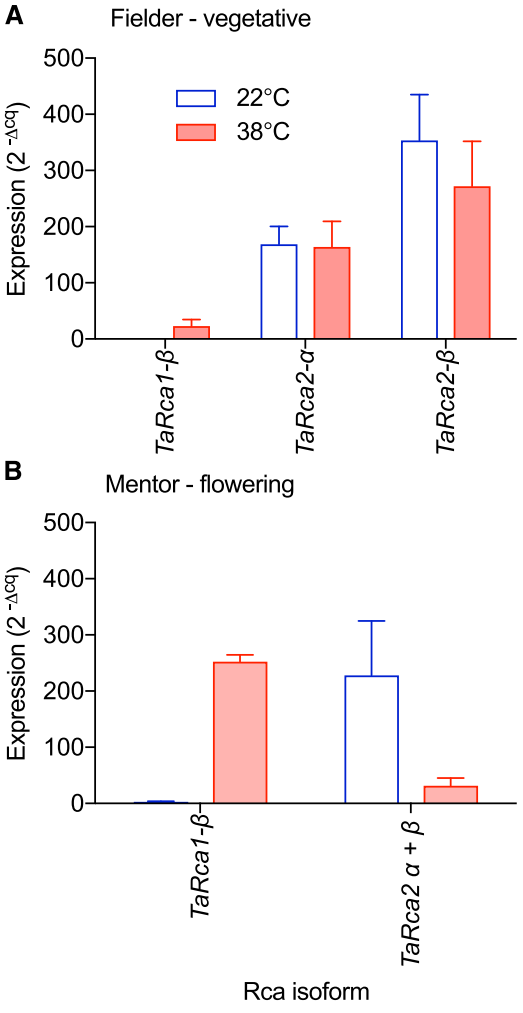

Figure 1. A comparison of gene expression of Rca isoforms extracted from wheat leaves either under control conditions (22°C day/night) or after heat treatment. A, The spring wheat 'Fielder' harvested during the vegetative stage with heat treatment being 38°C/22°C for two diurnal cycles. B, The winter wheat 'Mentor' harvested during the flowering stage with heat treatment being 36°C/22°C for seven diurnal cycles. Gene expression analysis via reverse transcription quantitative PCR (qPCR) for cv Fielder used primers specific to the wheat *TaRca1-β* gene and *TaRca2-α* and *TaRca2-β* spliced variants, whereas for cv Mentor, primers were nonspecific for the *TaRca2* spliced variants. Expression values are means ± SD of three or more biological replicates.

variants, went from undetectable expression levels at control temperature to a substantial level under the heat treatment. Even so, *TaRca1-β* expression was well below expression of the *TaRca2* spliced variants. However, when the winter wheat 'Mentor' was exposed to a heat treatment of 36°C during the light period for 7 d during its flowering stage, *TaRca1-β* expression increased more dramatically than for cv Fielder in the vegetative stage (Fig. 1B). For cv Mentor, there was a small amount of *TaRca1-β* detected under control conditions but a highly responsive increase in *TaRca1-β* with heat exposure, approaching expression levels of the *TaRca2* spliced variants observed under control conditions and accompanied by an almost as pronounced decline in expression of the *TaRca2* spliced variants. Irrespective of the differences in isoform expression profiles between cv Fielder and Mentor, which could have been due to genotypic, developmental, or heat treatment variation, in both cases it seems that heat induced the expression of the *TaRca1-β* gene, implying that the TaRca1-β protein is involved in the heat response of wheat. Similar to cv Mentor, *TaRca1-β* gene induction by heat at flowering was observed in other winter wheat cultivars (Supplemental Fig. S1).

To establish if the observed changes in the expression profiles of the various Rca isoforms due to heat had an effect on the activity and heat stability of the Rca holoenzyme, the protein was extracted and isolated from leaves. Absolute rates of Rubisco activation velocity by Rca measured at 25°C (V_{25}) were lower for Rca extracted from cv Mentor heat-treated extracts compared with all others (Fig. 2A; Table 1). The cv Mentor heat-treated extracts had potentially more degradation of Rca purified from the leaf, evident from additional gel bands just below the expected position of the β-isoforms (Supplemental Fig. S2), which could have contributed to lower in vitro activity. Rubisco contamination of leaf-extracted Rca samples did not influence the results, as no Rubisco activity was detected in assays containing Rca extracts minus the addition of the Rubisco substrate (Fig. 2A). Determination of the T_m, using both enzymatic velocity of preheated protein and DSF, showed that T_m did not significantly differ for cv Fielder or Mentor control samples at the different developmental stages (Fig. 2, B and C; Table 1). Based on enzymatic velocity, there was a significant increase in T_m for the heat-treated cv Mentor but not the cv Fielder extracts. Using DSF, heat-treated cv Fielder had a significantly higher T_m than the control treatments and heat-treated cv Mentor was significantly higher again, with the latter having a T_m 3.5°C above the control (Fig. 2; Table 1).

Recombinant and native Rca isoforms were expressed and purified to test if induction of *TaRca1-β* expression and the associated increase in Rca thermal stability observed in heat-treated leaves were in fact due to TaRca1-β being a more thermostable variant of Rca than TaRca2-β or TaRca2-α. The β-isoform of Rca from rice (OsRca-β) was used as a reference for heat stability, as rice is a tropical species unlike temperate wheat. Of note, the consistency between T_m determined by enzymatic velocity and DSF, particularly for recombinant protein (Table 1), suggests that DSF is a good surrogate for determining the loss of enzyme functionality and not just loss of structural integrity of Rca. The T_m of the TaRca2 α- and β-isoforms were not significantly different from one another and independent of the T_m method used. OsRca-β had a $T_m > 7$°C above the TaRca2 spliced variants (Fig. 3; Table 1). Of interest, the TaRca1-β isoform was indeed a heat-stable variant of Rca for wheat, to the extent that its T_m was greater than 7°C above that of both TaRca2 variants and within 1°C of that of the rice OsRca-β isoform. The V_{25} of TaRca1-β, however, was significantly less than the velocity of the other wheat and rice Rca isoforms, which had similar V_{25}.

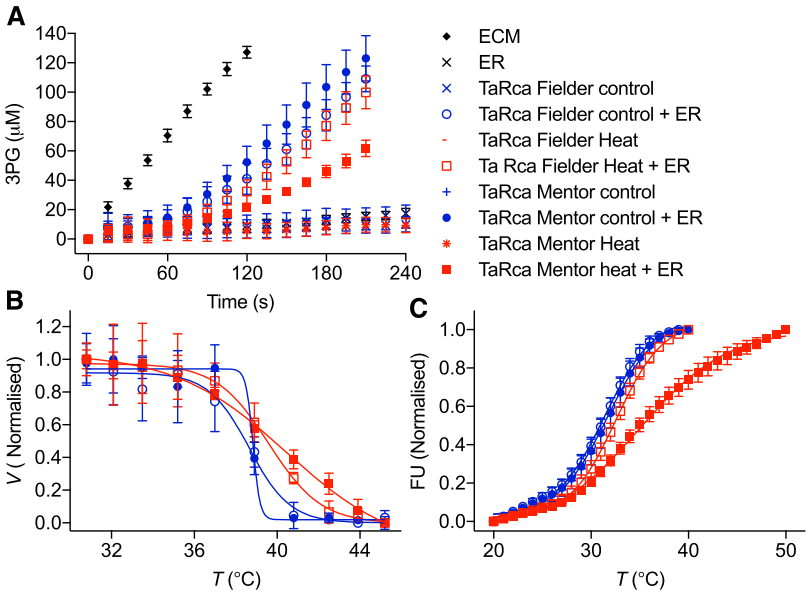

Figure 2. Analysis of Rubisco interactions with Rca extracted from wheat leaves either under control conditions or after heat treatment. A, Rubisco activation velocity by Rca at 25°C. The production of 3-phosphoglycerate (3PG) by Rubisco primed with CO_2 and Mg^{2+} (ECM), Rubisco inhibited by its substrate RuBP (ER), ER Rubisco in the presence of Rca, and Rca extracts with no Rubisco present enabled the determination of V_{25}. B, Temperature-dependent Rubisco activation by Rca. Rca was incubated for 10 min in the presence of 0.2 mM ATP at the indicated temperatures prior to assaying at a standard 25°C and normalized to the fastest velocity achieved for each sample. C, DSF for Rca. Samples were heated at 1°C min^{-1}, and fluorescence units (FU) normalized to the maximum value were recorded. Values are means ± SD of three biological replicates. Curves are the ordinary least-squares fit of a Boltzmann sigmoidal equation (Eq. 1). V_{25} and T_m are presented in Table 1.

Table 1. *The initial V_{25} (mol ECM regenerated $min^{-1} \times 10^{-3}$ mol^{-1} Rca) and the thermal midpoint at which half of Rca velocity or structural stability is lost (T_m) calculated from Rca activation assays (V) or differential scanning fluorimetry (DSF)*

Values are means ± SD of four or more experimental replicates. The preincubation heating of Rca was undertaken in the presence of 0.2 mM ATP or the absence of ATP for selected variants as indicated. Different letters indicate significant differences between variants at $P \leq 0.05$ determined using a one-way ANOVA and Tukey's multiple comparison test with leaf-extracted and recombinant protein analyzed separately. Dashes indicate that no measurements were taken.

Source	Variant	0.2 mM ATP			No ATP
		V_{25}	T_m V	T_m DSF	T_m V
			°C	°C	°C
Leaf	cv Fielder control	55 ± 6 a	38.6 ± 0.2 a	31.4 ± 0.4 a	–
	cv Fielder heat	63 ± 6 a	39.5 ± 0.5 a	32.6 ± 0.4 b	–
	cv Mentor control	56 ± 8 a	38.5 ± 0.3 a	31.6 ± 0.9 a	–
	cv Mentor heat	31 ± 5 b	40.3 ± 0.9 b	35.2 ± 1.3 c	–
Recombinant	TaRca2-α	52 ± 5 a,b	35.3 ± 0.2 a	34.6 ± 0.4 a	–
	TaRca2-β	59 ± 6 a	34.8 ± 0.5 a	34.4 ± 0.4 a	29.1 ± 0.3
	TaRca1-β	26 ± 2 c	42.0 ± 0.2 b	41.4 ± 0.2 b	35.4 ± 0.6
	OsRca-β	51 ± 7 a,b	42.5 ± 0.4 b	42.1 ± 0.3 c	37.6 ± 0.4
	TaRca2-β-11AA	49 ± 8 a,b	42.4 ± 0.5 b	41.5 ± 0.4 b	36.3 ± 0.4
	TaRca2-β-8AA	45 ± 5 b	40 ± 0.4 c	39.1 ± 0.7 d	33.1 ± 0.3
	TaRca2-β-3AA	80 ± 7 d	37.4 ± 0.4 d	36.6 ± 0.4 e	30.3 ± 0.6

Sequence alignments and protein structural modeling were used as tools to determine the residues that are conserved in thermostable variants of Rca so that mutations could be made to the heat-sensitive TaRca2-β in an effort to raise its thermal stability (Fig. 4). Mutations were proposed based on protein alignment of TaRca2-β with thermostable TaRca1-β and OsRca-β as well as Rca consensus sequences from cold- and warm-adapted species. The cold and warm consensus sequences were generated by aligning Rca sequences taken from public databases of species we classified as endemic to cold or warm environments. The species used for these alignments are named in "Materials and Methods," and the alignments are given in Supplemental Figures S3 and S4. The first TaRca2-β mutant generated had 11 amino acid substitutions (TaRca2-β-11AA) based on differences between the TaRca2-β and TaRca1-β sequences with the criteria that TaRca1-β matched the warm species consensus sequence and was different from the cold species consensus sequence. A second mutant was generated based on TaRca2-β-11AA but with the additional criterion that if any of the OsRca-β residues at these 11 amino acid mutation sites matched the corresponding TaRca2-β or the cold species consensus sequence, then the original TaRca2-β residue was reinstated. This reduced the number of mutations by three, leading to an eight-amino acid mutant (TaRca2-β-8AA). Finally, to test the potential importance of subunit interaction on overall Rca thermostability, modeling of the Rca

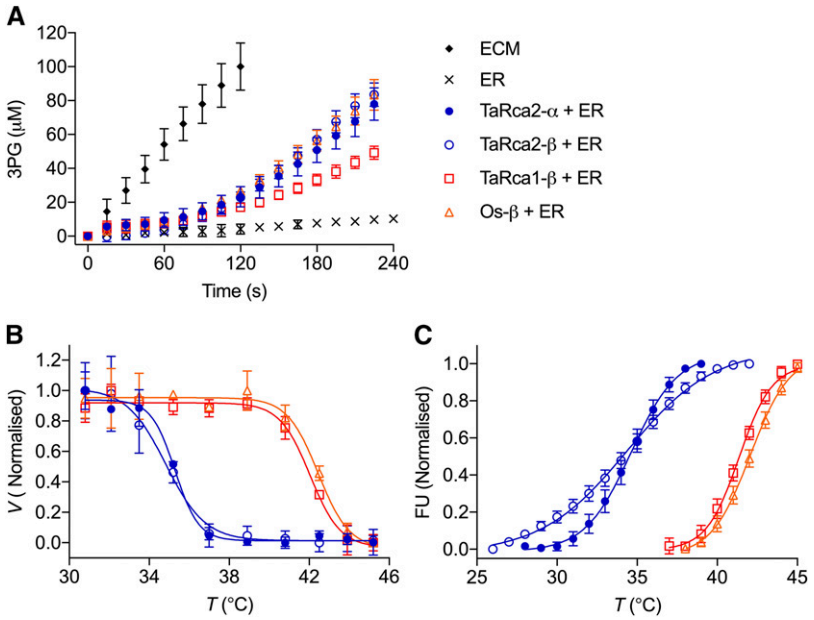

Figure 3. Analysis of Rubisco interactions with variants of Rca. Included in the analyses were recombinant TaRca2-α, TaRca2-β, TaRca1-β, and OsRca-β. A, Rubisco activation velocity by Rca at 25°C. Experiments consisted of 1.6 ± 0.2 μM Rca protomer added to 0.2 ± 0.05 μM Rubisco active sites inhibited by RuBP (ER). B, Temperature-dependent Rubisco activation by Rca. Rca was incubated for 10 min in the presence of 0.2 mM ATP at the indicated temperatures prior to assaying at a standard 25°C, and values are normalized to the fastest velocity achieved. C, DSF. Samples were heated at 1°C min^{-1}, and fluorescence units (FU) normalized to the maximum value were recorded. Values are means ± SD of four experimental replicates. Curves are the ordinary least-squares fit of a Boltzmann sigmoidal equation (Eq. 1). The calculated initial V_{25} and T_m are presented in Table 1.

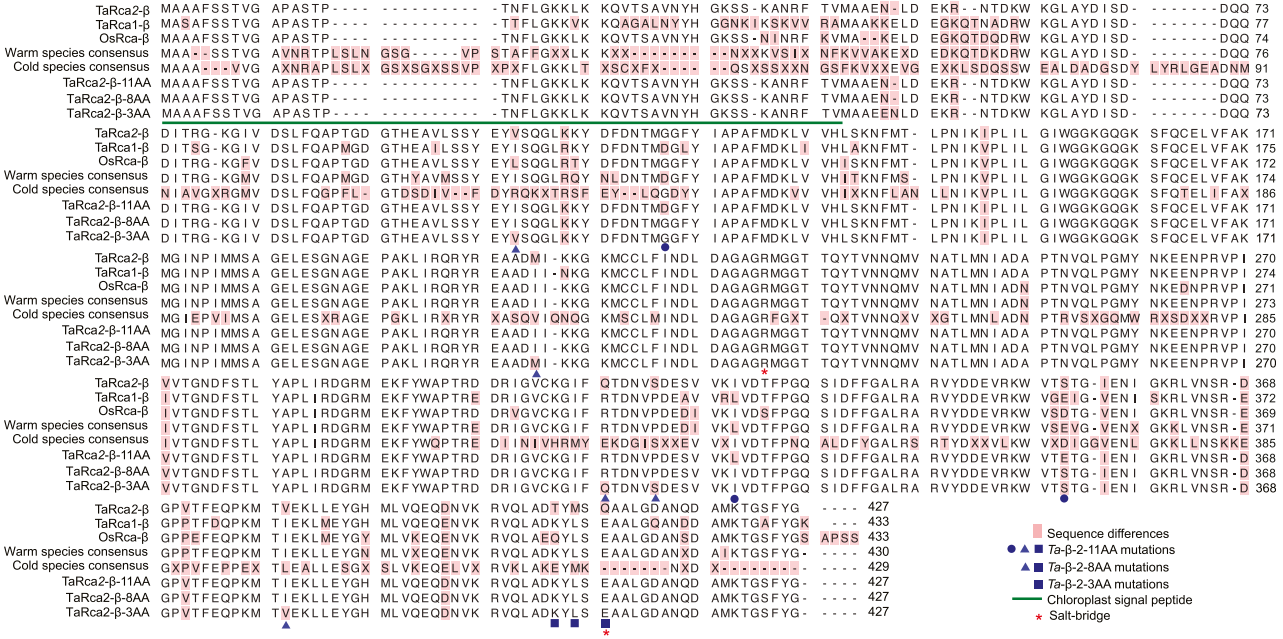

Figure 4. Rca sequence alignment. Included in the alignment are TaRca2-*β*, TaRca1-*β*, OsRca-*β*, the consensus sequences of warm- and cold-adapted species, and a mutated sequence of TaRca2-*β* with 11 amino acid substitutions (TaRca2-*β*-11AA), eight amino acid substitutions (TaRca2-*β*-8AA), and three amino acid substitutions (TaRca2-*β*-3AA). The consensus sequences were generated from alignments of eight and nine species endemic to warm and cold environments, respectively. The mutations made to TaRca2-*β*-11AA, with positions indicated by blue circles, triangles, and squares, were selected based on the TaRca1-*β* sequence with the criteria that TaRca1-*β* matched the warm-adapted species' consensus and was different from the cold-adapted species' consensus. The mutations made to TaRca2-*β*-8AA, with positions indicated by blue triangles and squares, were selected based on TaRca2-*β*-11AA but with the additional criterion that if any of the OsRca-*β* residues at these 11 amino acid mutation sites matched the corresponding TaRca2-*β* or the cold-adapted species' consensus sequence, then the original TaRca2-*β* residue was reinstated. The mutations made to TaRca2-*β*-3AA, with positions indicated by blue squares, were selected based on structural modeling that showed the final three substitutions to be in close proximity to adjacent monomers. The red asterisks indicate the salt bridge formed between adjacent monomers as predicted by protein modeling of TaRca2-*β*-3AA. Residue differences among the sequences are highlighted in red. The chloroplast signal peptide, which was not included in the analysis, is underlined in green.

hexamer was performed and this identified the final three C-terminal mutations of the TaRca2-*β*-11AA variant to be in close proximity to adjacent monomers (Supplemental Fig. S5). Therefore, a variant was generated with only the three final substitutions (TaRca2-*β*-3AA; Fig. 4).

Temperature response curves of Rubisco activation by Rca showed that the TaRca2-*β*-11AA, TaRca2-*β*-8AA, and TaRca2-*β*-3AA mutants did have greater thermal stability than the heat-sensitive TaRca2-*β* wild-type isoform (Fig. 5; Table 1). In fact, TaRca2-*β*-11AA had a T_m of 41.5°C to 42.4°C, similar to that of the TaRca1-*β* and OsRca-*β* thermostable isoforms, and, again, greater than 7°C above that of TaRca2-*β*. Whereas TaRca2-*β*-8AA had improved thermal stability, with a T_m of 39.1°C to 40°C depending on experimental method, it was intermediate between TaRca2-*β* and the other thermostable isoforms, increasing TaRca2-*β* T_m by 5.2°C to 6.1°C. Similarly, the TaRca2-*β*-3AA mutant had a T_m significantly higher than that of the TaRca2-*β* wild-type isoform but less than that of the TaRca2-*β*-8AA and TaRca2-*β*-11AA variants. This indicates that the extra residue substitutions for each of the three TaRca2-*β* mutant variants provided a further significant contribution in promoting heat stability of Rca in wheat. The TaRca2-*β*-11AA variant had similar, the TaRca2-*β*-8AA variant had slightly reduced, and the TaRca2-*β*-3AA variant had significantly faster V_{25} than the TaRca2-*β* wild-type isoform, and thus no relationship, or tradeoff, was found between thermal stability and kinetic efficiency for the mutants under the standard conditions measured. The improvement in T_m of the variant with 11 residues modified occurred irrespective of whether the TaRca2-*β* or TaRca2-*α* spliced isoform was mutated (Supplemental Fig. S6).

As ATP is known to influence Rca thermostability in vitro (Henderson et al., 2013; Keown and Pearce, 2014), the effect of adding no ATP when incubating Rca samples at the varying temperatures was assessed (Fig. 6; Table 1). A lack of ATP in the sample reduced the T_m for all Rca variants significantly. The fall in T_m in the absence of ATP was quite substantial and ranged from 4.9°C for OsRca-*β* to 7.1°C for TaRca2-*β*-3AA, demonstrating that T_m calculations and thus thermal

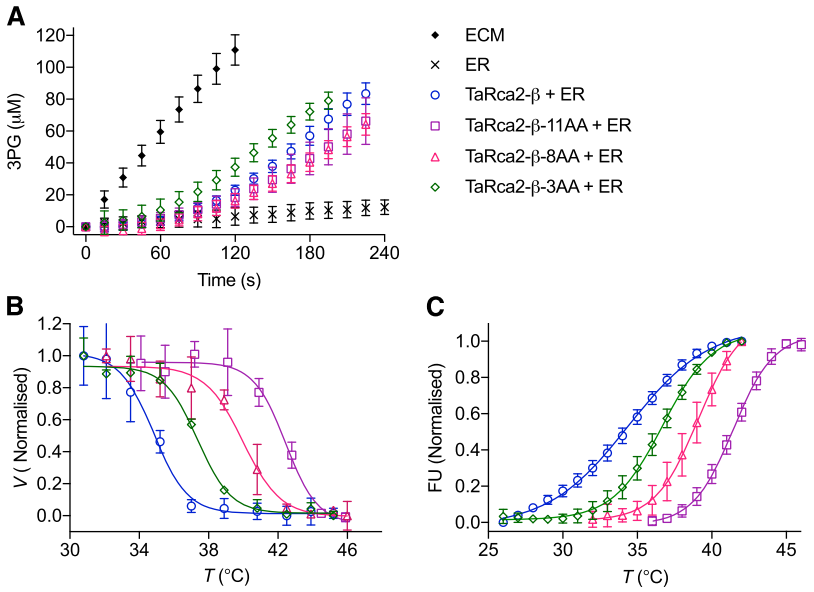

Figure 5. Analysis of Rubisco interactions with recombinant TaRca2-β and the TaRca2-β-11AA, TaRca2-β-8AA, and TaRca2-β-3AA mutants. A, Rubisco activation velocity by Rca at 25°C. B, Temperature-dependent Rubisco activation by Rca. C, DSF. Values are means ± SD of four or more experimental replicates. Curves are the ordinary least-squares fit of a Boltzmann sigmoidal equation (Eq. 1). V_{25} and T_m are presented in Table 1.

stability of Rca from wheat are susceptible to the presence of nucleotide when the enzyme is heated.

Models suggested that TaRca2-β monomers form a hydrogen bond between Gln-409 and a conserved Arg-226 in the pore loop of an adjacent monomer at two positions, whereas the Glu-409 and Arg-226 residues of TaRca1-β formed salt bridges at four positions (Fig. 7). Similarly, the TaRca2-β-3AA variant was predicted to form salt bridges at four sites of the hexameric complex between Glu-409 and Arg-226. To further test subunit interaction of the Rca oligomer, an inactive mutant was created with a K157Q substitution in the Walker A motif, a mutation resulting in minimal Rca activity while still allowing the formation of oligomeric complexes (Fig. 8). When titrating wild-type TaRca2-β or TaRca2-β-3AA with the K157Q inactive mutant and measuring the velocity of Rubisco activation within 1 min of mixing, the velocity of the mixture closely followed a binomial distribution equation assuming a hexameric complex in which the incorporation of one inactive K157Q monomer impaired the entire activity of the complex, following the formula $V = (1 - X)^{(6+6)} * X * (1 - X)^{(6-1)}$ (Stotz et al., 2011), where V is Rca activation velocity and X is the fraction of K157Q subunits added (Fig. 8C). In other words, the fact that we observed the binomial distribution suggests that the isoforms were interacting to form heterooligomeric complexes, and the fact that this occurred within 1 min of mixing the separate isoforms suggests that complexes were forming on a time frame of seconds. Mixing of TaRca1-β with the inactive TaRca2 K157Q mutant at 25°C showed poisoning of a formed complex with a significant 50% decline in total TaRca velocity. However, when incubated for 10 min at 40°C, no significant poisoning was observed, with TaRca1-β maintaining 89% of its velocity (Fig. 8D).

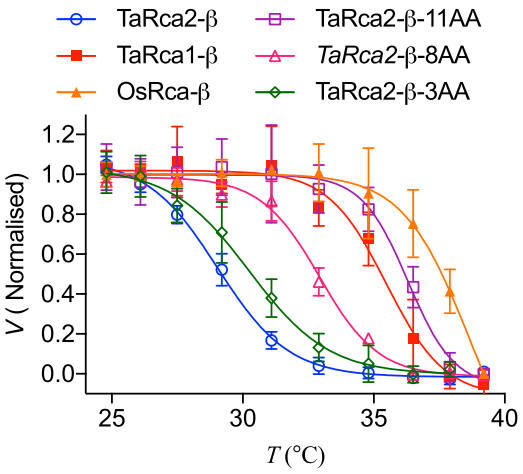

Figure 6. Temperature-dependent Rubisco activation by variants of Rca without ATP nucleotide. Rca variants assayed were recombinant TaRca2-β, TaRca1-β, OsRca-β, and TaRca2-β-11AA, TaRca2-β-8AA, and TaRca2-β-3AA mutants. Rca was incubated for 10 min at the indicated temperatures in the absence of ATP prior to assaying at a standard 25°C. Values are normalized to the fastest velocity achieved. Values are means ± SD of four experimental replicates. Curves are the ordinary least-squares fit of a Boltzmann sigmoidal equation (Eq. 1). T_m are presented in Table 1.

DISCUSSION

Heat stress induced the *TaRca1-β* gene, and Rca extracted from these leaves had reduced V_{25} and increased T_m. Recombinant Rca experiments showed TaRca1-β to have reduced V_{25} and higher T_m than that of the TaRca2 variants, consistent with the characteristics of Rca isolated from heat-treated wheat leaves. It therefore seems clear that one mechanism wheat has evolved in regard to heat response is to induce the expression of a thermally stable Rca isoform (TaRca1-β),

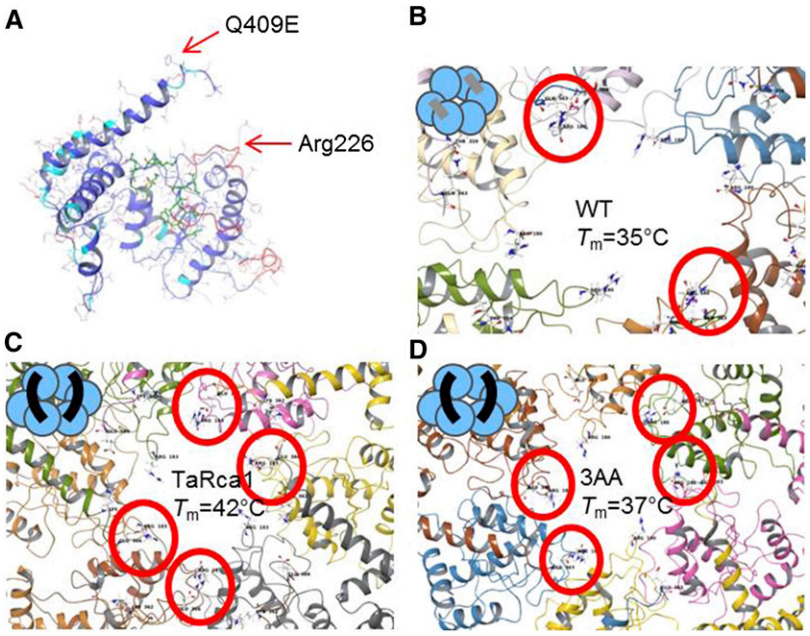

Figure 7. Structural analysis of Rca variants. A, Structural model of the wheat Rca monomer indicating the position of the Q409E substitution and a conserved Arg-226 residue in pore loop 2. Residues colored green indicate the nucleotide-binding region. B to D, Bottom views through the hexamer central pore of TaRca2-β wild type (WT; B), TaRca1-β (C), and TaRca2-β-3AA variants (D). B, Modeling showing that Gln-409 at the C-terminal region forms a hydrogen bond with Arg-226 in pore loop 2 of an adjacent monomer in two instances in the wild-type complex. C and D, Glu-409 forms a salt bridge with Arg-226 of an adjacent monomer in four instances in TaRca1-β and the TaRca2-β-3AA variant. Cartoon illustrations of the hydrogen bonding (gray) and the salt bridge (black) between monomers of the hexameric complex are given in the top left corners. Interacting residues forming the hydrogen or salt bridge are circled in red. The Q409E and Arg-226 positions are in relation to sequence alignments as presented in Figure 4.

which presumably enables photosynthesis to continue at higher temperatures, considering that the heat-labile nature of Rca is a major limitation on photosynthesis at higher temperatures for many plant species, including wheat (Feller et al., 1998; Crafts-Brandner and Salvucci, 2000; Sage et al., 2008; Perdomo et al., 2017; Kumar et al., 2019). The fact that other species such as cotton (*Gossypium hirsutum*) and maize (*Zea mays*; Sánchez de Jiménez et al., 1995; DeRidder and Salvucci, 2007) also induce specific isoforms of Rca in response to heat stress suggests convergent evolution of the induction of heat-stable Rca isoforms in response to heat. Why some species have evolved heat-inducible thermostable Rca variants whereas other species like rice have relatively thermostable variants expressed independent of temperature is intriguing. The reduced velocity observed for TaRca1-β might suggest that there is a penalty to enzymatic catalysis for the heat-stable variant. We have previously argued that thermostability comes at a cost to catalytic efficiency, finding that leaf-extracted Rca from *O. australiensis* was more thermostable but had reduced activity relative to Rca of cultivated rice (Scafaro et al., 2016). However, more recently, *A. tequilana* Rca was found to have a much higher thermostable Rca isoform as well as faster enzymatic velocity than rice Rca (Shivhare and Mueller-Cajar, 2017). Here, the fact that rice OsRca-β and the TaRca2-β-11AA mutant had nonsignificant differences in velocity compared with TaRca2-β when measured at a standard 25°C and yet were far superior in heat stability (Figs. 3 and 5) implies that there is not necessarily an intrinsic tradeoff between thermal stability and enzymatic velocity for Rca.

Irrespective of the Rca variant, the presence or absence of ATP influenced the thermal stability of the enzyme. It is well known that ATP helps in the formation of the Rca multimeric complex and that increasing ATP concentrations can lead to the formation of larger, more active complexes (Wang et al., 1993, 2018). Furthermore, ATP has been shown to provide thermal stability to Rca, attributed to the role of ATP in self-association (Crafts-Brandner et al., 1997; Salvucci et al., 2001; Barta et al., 2010; Keown and Pearce, 2014). We show here that ATP thermal protection of Rca also occurs for wheat and that this ATP protection is independent of the intrinsic heat stability of Rca (Table 1; Fig. 7).

The most heat-labile TaRca2-β wheat isoform had a T_m of 34°C, similar to the temperature at which photosynthesis in wheat becomes impaired (Yamasaki et al., 2002; Silva-Pérez et al., 2017). We were able to improve the enzymatic thermostability of TaRca2-β by 7.6°C with as little as 11 residue substitutions. Reducing the number of substitutions by three reduced the benefit to T_m to 5.2°C. Thus, a 28% reduction in the number of mutations resulted in a similar reduction of 32% in benefit to thermostability. Furthermore, reducing the number of mutations to three based on modeling analysis increased T_m relative to wild-type Rca by 2°C, a 72% reduction in benefit from a 73% reduction in the mutations present in TaRca2-β-11AA. It therefore seems likely that a cumulative interaction of multiple residue sites is required to gain thermostability. However, whether each of the 11 residue substitutions contribute equally to the greater than 7°C increase in T_m remains unclear and awaits further examination. The mutants we have generated provide invaluable information about parts of the primary Rca protein structure related to thermostability. Eight of the 11 mutations for TaRca2-β-11AA occur between positions 310 and the C terminus at position 427 (Fig. 4), regions associated with Rubisco-Rca and Rca-Rca interactions (Li et al., 2005, 2006;

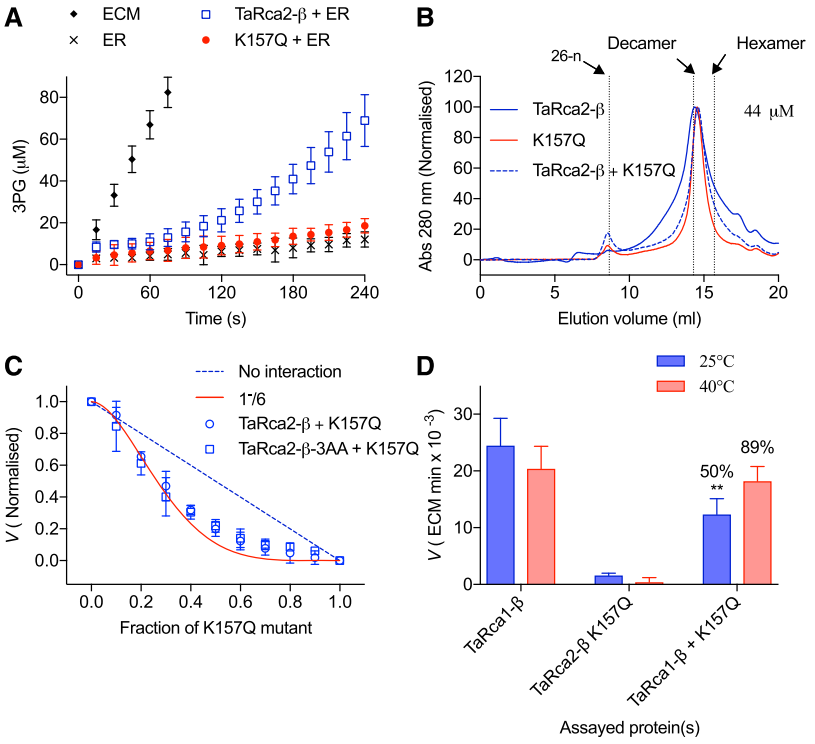

Figure 8. Enzyme interaction studies of TaRca2-β and TaRca1-β variants with the inactive TaRca2-β K157Q mutant. A, The production of 3PG by reactivated Rubisco in the presence of TaRca2-β (TaRca2-β + ER) and the inactive mutant (K157Q + ER), demonstrating that the TaRca2-β K157Q mutant is essentially inactive. Values are means ± SD of four experimental replicates. B, Gel-filtration chromatogram showing homooligomeric and heterooligomeric complexes of TaRca2-β, TaRca2-β K157Q, and when the two are mixed at a concentration of 44 μM. The chromatogram is normalized to 100 at the maximum peak height. C, Observed Rca activation velocity normalized to wild-type velocity when titrating different fractions of an inactive TaRca2-β K157Q mutant with the wild-type complex (circles) or the TaRca2-β-3AA variant (squares), measured within 1 min after mixing. Values are means ± SD of three experimental replicates. The red solid curve represents a binomial distribution model, $V = (1 - X)^{(6+6)} * X * (1 - X)^{(6-1)}$, predicting loss of function from incorporation of a single inactive monomer into a hexameric complex. The dashed blue line represents a decline if either no heterooligomeric complexes were formed or velocity declined proportionally to inactive monomers. D, Activation velocity of 1.6 μM TaRca1-β, 1.6 μM TaRca2-β K157Q mutant, and 1.6 μM of both mixed. ATP (0.2 mM) was added to samples before incubating for 10 min at either 25°C or 40°C. Values are means ± SD of five experimental replicates. The percentage decline in velocity relative to TaRca1-β by itself is reported above the mixed samples. **, Significant at $P < 0.001$ determined by a nonpaired Student's t test.

Stotz et al., 2011). Four of the mutations were in the final 50 residues of the C terminus. Structural analysis of the Rca complex that we (Fig. 7) and others have performed identified the C terminus of each monomer as being in close proximity to an adjacent Rca monomeric nucleotide-binding pocket, involved in complex formation through allosteric interaction between these adjacent subunits (Stotz et al., 2011). Interestingly, three of the mutations are located within three residue positions from the TaRca2-β Tyr-406 residue, which is conserved across species and essential for ATP hydrolysis and Rubisco activation functionality, presumably through allosteric interactions, as Tyr-406 is not in close proximity to the Walker A or B nucleotide-binding sites of individual monomers (Portis et al., 2008; Stotz et al., 2011). Indeed, modeling predicts that the Gln-to-Glu substitution we made at position 409, the final mutation of TaRca2-β-11AA at the C terminus, forms a salt bridge with a conserved Arg (Arg-226) in pore loop 2 of an adjacent monomer (Fig. 7). Of note, substitution of the corresponding Arg-226 residue in tobacco (*Nicotiana tabacum*) to an Ala had minimal effect on ATP hydrolysis and activation velocity of tobacco Rca (Li et al., 2006). Potentially, the C terminus and in particular the Q409E mutation we modeled may be important in relation to thermostability through its contribution to allosteric subunit interaction near the nucleotide-binding pocket.

However, three observations must be considered: (1) TaRca1-β and TaRca2-β-3AA had the same modeled salt bridge yet had significantly different T_m values; (2) although the TaRca2-β-3AA variant had a significant increase in T_m relative to the wild-type isoform, it was significantly less than the TaRca2-β-8AA and TaRca2-β-11AA variants, which had mutations that modeling analysis did not show to be in proximity to adjacent monomers; and (3) subunit interaction studies we performed (Fig. 8) demonstrated that monomers of Rca are

freely interchangeable with the oligomeric complex within a time frame of seconds, as others have observed (Wang et al., 2018), irrespective of differences in the modeled C-terminal subunit interactions. These three findings imply that the stability of individual monomers and not the stability of the oligomer is the greatest contributor to Rca thermostability. Previous findings by heat poisoning experiments of thermally sensitive subunits (Shivhare and Mueller-Cajar, 2017) and monomers forming inactive aggregates at high temperatures (Barta et al., 2010) support the conclusion that formation and not stabilization of the oligomeric complex is what is susceptible to thermal damage. Following this argument, we postulate that the ATP-dependent improvement in thermostability that we and others have observed may represent improvements to the stability of monomers with bound ATP, potentially through binding interactions of divalent cations, as postulated previously (Henderson et al., 2013), rather than improvements due to ATP facilitating the stabilization of the multimeric complex. Similar to the poisoning experiments of Shivhare and Mueller-Cajar (2017), we demonstrate that the heat-sensitive TaRca2 (as the K157Q inactive mutant) forms heterooligomeric complexes with the thermally stable TaRca1-β variant at 25°C but not at 40°C, above the T_m of TaRca2 but below the T_m of TaRca1-β, as TaRca2 would have aggregated out of solution at 40°C, leaving only functional TaRca1-β homooligomer complexes (Fig. 8D). This result implies that when mixing isoforms of varying thermostability, the complex will take on the thermal and velocity properties equal to the isoform in the mix that has a T_m above the heat exposure temperature. The K157Q titration experiment supports wheat Rca being functional as a hexamer despite forming oligomers of varying number due to concentration-dependent self-association and the loss of hexametric complex functionality due to a single inactive subunit within the complex; future characterization of the Rca-Rubisco interaction should resolve why this is so. Interestingly, TaRca2-β-8AA and TaRca1-β had slower, TaRca2-β-11AA had similar, and TaRca2-β-3AA had faster V_{25} relative to the TaRca2-β wild type, showing multifaceted mutational influence on Rca activation velocity.

Previous mutations to Rca from Arabidopsis (*Arabidopsis thaliana*) identified eight residues that led to an improvement in thermostability (Kurek et al., 2007) but not in residues that correspond to any of the sites we mutated in this study (Supplemental Fig. S7). Furthermore, 19 residue differences in the thermally superior Rca from *O. australiensis* relative to the sequence of rice (Scafaro et al., 2016) do not correspond to differences for 10 of the 11 residues we mutated. However, considering that we based our mutation selection on the differences in consensus sequences between warm- and cold-adapted species, it does seem that at least some amino acids conferring thermostability are conserved among the Rca of warm-adapted species. Furthermore, improving thermostability was proportional to the number of mutations we made, suggesting that each mutation provides an additive effect to the thermostability of the enzyme. Therefore, we suggest a mechanism for improving the thermostability of Rca, which is to generate mutations based on conserved residues in species from warmer habitats and make multiple rather than single mutations. The isoform and residues related to heat stabilization of Rca for wheat that we have discovered provide a mechanism to engineer wheat with superior photosynthetic performance during heat stress. We envisage either manipulating Rca gene regulation to overexpress the thermotolerant endogenous TaRca1-β isoform or genetically editing TaRca2-β isoforms to incorporate the stabilizing mutations as two possible mechanisms for improving wheat tolerance to heat stress. The ultimate benefit to heat stress tolerance of wheat can only be determined through in planta studies, which we are currently exploring.

MATERIALS AND METHODS

In Situ Heat Treatment Experiment

Wheat (*Triticum aestivum*) 'Fielder' or 'Mentor' seeds were wetted and placed on germination paper with stratification for 1 week at 4°C, followed by sowing in 17-cm-diameter pots with potting soil. Pots were placed in a growth chamber with a 12-h photoperiod at a constant 22°C and 300 μmol m^{-2} s^{-1} photosynthetically active radiation. For cv Fielder, 35 d after sowing, half of the pots were relocated to an adjacent growth chamber with a 38°C light period temperature. At 38 d after sowing, all healthy leaf material was harvested in the middle of the light period and snap frozen in liquid N_2 before being stored at −80°C until further use. For cv Mentor, the heat treatment began when the plants were flowering, and heat treatment was 7 d with a light period temperature set to 36°C. To determine Rca gene expression, reverse transcription qPCR was performed on leaf material using primers and a PCR cycle as outlined in Supplemental Table S1.

Rca and Rubisco Leaf Extraction and Purification

Protein was extracted from the leaves grown under standard physiological conditions as described above. Frozen leaf tissue was ground into a fine powder using liquid N_2 and a mortar and pestle. While on ice, leaf powder was added to and repeatedly vortexed in an extraction buffer consisting of 100 mM Tris, pH 8, 1 mM EDTA, 7.5 mM $MgCl_2$, 2 mM DTT, 1 mM ATP, 2% (w/v) polyvinylpolypyrrolidone, and protease inhibitor cocktail, before being passed through a single layer of Miracloth and Lingette Gaze to remove solid matter. The sample was centrifuged at 24,000*g* for 20 min at 4°C, and supernatant was kept. Saturated ammonium sulfate was added to the sample until reaching 35% (v/v), and the sample was kept on ice for 30 min before recentrifugation. For Rca purification, the pellet was resuspended in leaf extraction buffer minus polyvinylpolypyrrolidone, desalted in the same buffer using Sephadex PD-10 desalting columns, loaded onto a 1-mL HiTrap Q FF column (GE Healthcare) with a flow rate of 1 mL min^{-1}, and equilibrated with desalting buffer. A gradient of desalting buffer containing 0.5 mM KCl from 0% to 100% over 20 mL at a 1 mL min^{-1} flow rate was used to elute Rca, and fractions determined to contain protein by Bradford assay (Bio-Rad) were pooled and concentrated using 10-kD Cutoff Amicon concentrators (Merck) to a concentration of 2.2 ± 0.5 mg mL^{-1} and stored at −80°C until further use. For Rubisco purification, to the supernatant after the saturated ammonium sulfate precipitation step (35%, v/v) described above, additional saturated ammonium sulfate was added dropwise until the saturated ammonium sulfate concentration reached 60% (v/v) of the sample. The sample was slowly stirred at 4°C for 30 min before recentrifugation. The resulting pellet was suspended in a sample buffer of 100 mM Tricine, pH 8, and 0.5 mM EDTA and desalted into the same buffer using PD-10 desalting columns. Glycerol (20%, v/v) was added, and the sample was divided into aliquots, snap frozen, and stored at −80°C until further use.

Recombinant Protein Production

All Rca genes of interest were synthesized de novo (GENEWIZ) with codons for the 46 amino acids at the N terminus corresponding to the signal peptide deleted and codons for a six-amino acid His tag inserted just upstream of the stop codon. Genes were ligated into Novagen pET-23d+ vectors (Merck) before being transformed into BL21(DE3) Star *Escherichia coli* strain following standard procedures. Cultures of 0.5 L were grown in 2-L conical flasks and induced with 0.8 mM isopropylthio-β-galactoside at an OD_{600} of 0.8 to 1, then grown for a further 17 h at 20°C. Cells were lysed by sonication for 10 s for five cycles at 16-μm amplitude (Soniprep 150; MSE). Purification was performed using 5-mL HisTrap FF columns (GE Healthcare) following the manufacturer's instructions. Final Rca protein was desalted into a buffer containing 20 mM Tris, pH 8, 0.2 mM EDTA, 7.5 mM $MgCl_2$, 1 mM DTT, and 50 mM KCl, at a concentration of 2.2 ± 0.5 mg mL^{-1}, snap frozen, and stored at −80°C until further use. Rca protein concentration was determined using Bradford Reagent (Bio-Rad) with a BSA standard, and molar concentration was calculated using the molecular masses of 46,171 and 42,327 D for the TaRca2 α- and β-isoforms of wheat, respectively, 42,861 D for the TaRca1 β-isoform from wheat, and 43,093 D for the rice (*Oryza sativa*) β-isoform. Impurities in isolated Rca samples (Supplemental Fig. S8) were also accounted for when calculating Rca concentration by gel image analysis using ImageJ software (National Institutes of Health).

Rubisco Activation Assays

The ability of Rca to activate Rubisco was measured following the ADP-insensitive coupled-enzyme spectrophotometric method (Scales et al., 2014) with the following modified details. All reagents were purchased from Merck except for D-2,3-phosphoglycerate mutase, which was expressed and purified as previously outlined (Scales et al., 2014). The assay was scaled down to 100-μL reactions and measured on Coster 96-well flat-bottom polystyrene plates (Corning), heated to 25°C using an Eppendorf Thermomixer. In one set of wells, a reaction solution with a final volume of 80 μL was added consisting of N_2-sparged MilliQ water, 5% (w/v) polyethylene glycol-4000, 100 mM Tricine, pH 8, 10 mM $MgCl_2$, 10 mM $NaHCO_3$, 5 mM DTT, 2.4 units (μmol min^{-1}) of enolase, 3.75 units of phospho*enol*pyruvate carboxylase, 6 units of malate dehydrogenase, 0.2 mM 2,3-bis-phosphoglycerate, 4 units of D-2,3-phosphoglycerate mutase, 10 units of carbonic anhydrase, 4 mM phosphocreatine, 20 units of creatine phosphokinase, 2 mM ATP, and 0.8 mM NADH. In another set of wells, a final volume of 20 μL consisted of 0.2 ± 0.05 μM Rubisco active sites added to either (1) an activation solution (N_2-sparged MilliQ water, 20 mM Tricine, pH 8, 20 mM $NaHCO_3$, and 10 mM $MgCl_2$) to determine Rubisco total carbamylated activity (ECM) or (2) 4 mM RuBP (99% pure) for Rubisco substrate inhibition (ER). Two minutes prior to measurements, 4 μL of Rca was added to ER wells as a separate droplet from the Rubisco solution. Rca was not added to ER samples when measuring spontaneous baseline activity. Ten minutes after the addition of Rubisco, the contents of the reaction solution wells were added to the Rubisco-containing wells by multipipette, and measurements of absorbance at a wavelength of 340 nm were immediately made on an Infinate M200 Pro plate reader (Tecan) every 15 s over an 8-min period. Up to 10 samples were assayed simultaneously. The quantification of ECM regenerated reactions by Rca per minute (mol ECM $min^{-1} \times 10^{-3}$ mol^{-1} Rca) was calculated by the method outlined by Loganathan et al. (2016). The amount of Rubisco active sites added to the assay was determined from the slope of a linear regression through the data points corresponding to the first 60 s of 3-PG product generated from ECM samples and factoring in a wheat Rubisco reaction rate constant of 2.1 (Hermida-Carrera et al., 2016) at 25°C.

Gel-Filtration Chromatography

Rca in a 200-μL volume was loaded onto a Superose 6 10/300 GL column (GE Healthcare) equilibrated with two column volumes and eluted with Rca desalting buffer at 0.5 mL min^{-1} and 4°C. Size markers were generated by a standard curve using a Gel Filtration Calibration Kit HMW (GE Healthcare) following the manufacturer's instructions.

T_m Analysis

Prior to measuring the Rubisco activation velocity, 5 μL of 2.2 ± 0.5 mg mL^{-1} Rca sample (~44 μM Rca protomer) with or without 0.2 mM ATP added was placed in 4Titude PCR tubes (BIOKE) and heated on a Labcycler (SensoQuest) set at 38°C or different temperature dependent on Rca variant, with an 8°C temperature range over 12 positions. All tubes were initially heated for 2 min at 25°C followed by heating of individual tubes across the 8°C temperature range for 10 min. Tubes were then centrifuged at 4,000*g* for 5 min, and 4 μL of the preincubated Rca was added to activation assays as outlined above. Separately, the point at which Rca unfolded was determined by DSF as outlined previously (Niesen et al., 2007), with samples containing 11 ± 0.2 μM Rca protomer in a final volume of 20 μL made of 1:2,000 diluted Sypro Orange dye (Invitrogen), Rca desalting buffer, and 0.2 mM ATP. Samples were heated on a CFX384 qPCR instrument (Bio-Rad) at 1°C min^{-1} from 20°C to 50°C, and fluorescence was excited at 490 nm and emission was recorded at 610 nm at each temperature. An ordinary least-squares model was iteratively fit using the Boltzmann sigmoidal equation:

$$X = X_{Tmin} + (X_{Tmax} - X_{Tmin}) \Big/ 1 + exp^{(T_m - T/slope)} \quad (1)$$

where X is the activation velocity (V) or fluorescence units (FU), T *is the temperature in* °C, X_{Tmin} is the V or FU recorded at the minimum T, X_{Tmax} is the V or FU at maximum T , and slope is the steepness of the incline/decline. T_m was taken as the T at which X was at the midpoint between X_{Tmin} and X_{Tmax}, and the slope was set at an initial value of 2.

Protein Modeling and Sequence Alignments

Protein structural modeling was performed using Maestro molecular modeling software (Schrödinger). Initially, the protein sequences of TaRca2-β and variants minus the first 46 residues of the N terminus that make up the chloroplast signal peptide were folded into the 3D monomeric structure based on the Arabidopsis (*Arabidopsis thaliana*) Rca monomer crystal structure (Protein Data Bank entry 4W5W; http://dx.doi.org/10.2210/pdb4W5W/pdb). Following this, six of the derived wheat monomers were aligned into a hexameric structure using the tobacco (*Nicotiana tabacum*) hexamer (Protein Data Bank entry 3ZW6; http://dx.doi.org/10.2210/pdb3ZW6/pdb) as a template. The derived wheat hexameric structure was then optimized by minimizing the energy of the conformation in vacuum using standard software settings and 600 iterations.

All protein sequence alignments utilized the analysis software CLC Main Workbench V. 7.8.1 (Qiagen). Sequence alignments and the cold- and warm-adapted consensus sequences are presented in Supplemental Figures S3 and S4.

Statistical Analysis

All data and statistical analyses were carried out using Graphpad Prism 5.0 (GraphPad Prism Software) or R programming language (https://www.R-project.org/). All activation velocity experiments were repeated four or more times, and DSF experiments were repeated eight or more times. All values and error bars presented are means and SD of three or more experimental replicates. Significant differences in V_{25} and T_m of Rca between variants were determined using a one-way ANOVA and Tukey's multiple comparison test. Differences were considered significant at $P \leq 0.05$.

Accession Numbers

Sequence data from this article can be found in the GenBank/EMBL data libraries under the following accession numbers: AK455320.1 (TaRca2), AK455616.1 (TaRca1), BAA97584.1 (*Oryza sativa*), ANH11447.1 (*Oryza australiensis*), Q7X999.1 (*Larrea tridentate*), XP_009419709.1 (*Musa acuminate*), AAC62207.1 (*Datisca glomerata*), EOY07450.1 (*Theobroma cacao*), AAA78277.1 (*Nicotiana tabacum*), XP_016753736.1 (*Gossypium hirsutum*), NP_850321.1 (*Arabidopsis thaliana*), AFH35543.1 (*Brassica oleracea*), ABK25255.1 (*Picea sitchensis*), AAA34038.1 (*Spinacia oleracea*), XP_004305457.1 (*Fragaria vesca*), XP_015938754.1 (*Arachis duranensis*), XP_003580722.1 (*Brachypodium distachyon*), KFK41750.1 (*Arabis alpine*), and AAZ41846.1 (*Mesembryanthemum crystallinum*).

Supplemental Data

The following supplemental materials are available.

Supplemental Figure S1. Expression analysis of *TaRca1* and *TaRca2* genes in winter wheat cultivars during flowering and day temperatures of 22°C or 36°C.

Supplemental Figure S2. Leaf protein purity of Rubisco and Rca extracted from wheat leaves.

Supplemental Figure S3. Cold-adapted species sequence alignment.

Supplemental Figure S4. Warm-adapted species sequence alignment.

Supplemental Figure S5. 3D modeling of the Rca hexamer structure and location of mutations.

Supplemental Figure S6. Comparison of thermostability conferred by the 11 amino acid mutations on the two TaRca2 isoforms found in wheat.

Supplemental Figure S7. A comparison of amino acids in wheat, rice, and Arabidopsis Rca protein sequences associated with thermotolerance.

Supplemental Figure S8. SDS-PAGE analysis of recombinant protein purity.

Supplemental Table S1. PCR protocol and primers for wheat Rca gene expression analysis.

ACKNOWLEDGMENTS

We thank Anne Olivier from BASF Agricultural Solutions for wheat Rca gene analysis. We thank Iris de Beun, David De Vleesschauwer, Els Vercleyen, and Marianna Gabovicova from BASF Agricultural Solutions for vector construction. We thank Oliver Gutbrod, Svend Mattiesen, Michael Kohnen, and Michael Edmund Beck from Bayer CropScience Small Molecules Research for guidance with protein modeling.

Received April 5, 2019; accepted May 31, 2019; published June 12, 2019.

LITERATURE CITED

Barta C, Dunkle AM, Wachter RM, Salvucci ME (2010) Structural changes associated with the acute thermal instability of Rubisco activase. Arch Biochem Biophys **499:** 17–25

Busch FA, Sage RF (2017) The sensitivity of photosynthesis to O_2 and CO_2 concentration identifies strong Rubisco control above the thermal optimum. New Phytol **213:** 1036–1051

Carmo-Silva AE, Salvucci ME (2011) The activity of Rubisco's molecular chaperone, Rubisco activase, in leaf extracts. Photosynth Res **108:** 143–155

Carmo-Silva E, Scales JC, Madgwick PJ, Parry MA (2015) Optimizing Rubisco and its regulation for greater resource use efficiency. Plant Cell Environ **38:** 1817–1832

Crafts-Brandner SJ, Salvucci ME (2000) Rubisco activase constrains the photosynthetic potential of leaves at high temperature and CO_2. Proc Natl Acad Sci USA **97:** 13430–13435

Crafts-Brandner SJ, Van De Loo FJ, Salvucci ME (1997) The two forms of ribulose-1,5-bisphosphate carboxylase/oxygenase activase differ in sensitivity to elevated temperature. Plant Physiol **114:** 439–444

DeRidder BP, Salvucci ME (2007) Modulation of Rubisco activase gene expression during heat stress in cotton (Gossypium hirsutum L.) involves post-transcriptional mechanisms. Plant Sci **172:** 246–254

Feller U, Crafts-Brandner SJ, Salvucci ME (1998) Moderately high temperatures inhibit ribulose-1,5-bisphosphate carboxylase/oxygenase (Rubisco) activase-mediated activation of Rubisco. Plant Physiol **116:** 539–546

Henderson JN, Hazra S, Dunkle AM, Salvucci ME, Wachter RM (2013) Biophysical characterization of higher plant Rubisco activase. Biochim Biophys Acta **1834:** 87–97

Hermida-Carrera C, Kapralov MV, Galmés J (2016) Rubisco catalytic properties and temperature response in crops. Plant Physiol **171:** 2549–2561

Keown JR, Pearce FG (2014) Characterization of spinach ribulose-1,5-bisphosphate carboxylase/oxygenase activase isoforms reveals hexameric assemblies with increased thermal stability. Biochem J **464:** 413–423

Kumar RR, Goswami S, Singh K, Dubey K, Singh S, Sharma R, Verma N, Kala YK, Rai GK, Grover M, et al (2016) Identification of putative RuBisCo activase (TaRca1): the catalytic chaperone regulating carbon assimilatory pathway in wheat (*Triticum aestivum*) under the heat stress. Front Plant Sci **7:** 986

Kumar RR, Goswami S, Dubey K, Singh K, Singh JP, Kumar A, Rai GK, Singh SD, Bakshi S, Singh B, et al (2019) RuBisCo activase: A catalytic chaperone involved in modulating the RuBisCo activity and heat stress-tolerance in wheat. J Plant Biochem Biotechnol **28:** 63–75

Kurek I, Chang TK, Bertain SM, Madrigal A, Liu L, Lassner MW, Zhu G (2007) Enhanced thermostability of Arabidopsis Rubisco activase improves photosynthesis and growth rates under moderate heat stress. Plant Cell **19:** 3230–3241

Law RD, Crafts-Brandner SJ (2001) High temperature stress increases the expression of wheat leaf ribulose-1,5-bisphosphate carboxylase/oxygenase activase protein. Arch Biochem Biophys **386:** 261–267

Li C, Salvucci ME, Portis AR Jr (2005) Two residues of Rubisco activase involved in recognition of the Rubisco substrate. J Biol Chem **280:** 24864–24869

Li C, Wang D, Portis AR Jr (2006) Identification of critical arginine residues in the functioning of Rubisco activase. Arch Biochem Biophys **450:** 176–182

Loganathan N, Tsai YCC, Mueller-Cajar O (2016) Characterization of the heterooligomeric red-type Rubisco activase from red algae. Proc Natl Acad Sci USA **113:** 14019–14024

Mueller-Cajar O (2017) The diverse AAA^+ machines that repair inhibited Rubisco active sites. Front Mol Biosci **4:** 31

Nagarajan R, Gill KS (2018) Evolution of Rubisco activase gene in plants. Plant Mol Biol **96:** 69–87

Niesen FH, Berglund H, Vedadi M (2007) The use of differential scanning fluorimetry to detect ligand interactions that promote protein stability. Nat Protoc **2:** 2212–2221

Parry MAJ, Keys AJ, Madgwick PJ, Carmo-Silva AE, Andralojc PJ (2008) Rubisco regulation: A role for inhibitors. J Exp Bot **59:** 1569–1580

Parry MAJ, Reynolds M, Salvucci ME, Raines C, Andralojc PJ, Zhu XG, Price GD, Condon AG, Furbank RT (2011) Raising yield potential of wheat. II. Increasing photosynthetic capacity and efficiency. J Exp Bot **62:** 453–467

Perdomo JA, Capó-Bauçà S, Carmo-Silva E, Galmés J (2017) Rubisco and Rubisco activase play an important role in the biochemical limitations of photosynthesis in rice, wheat, and maize under high temperature and water deficit. Front Plant Sci **8:** 490

Portis AR Jr (2003) Rubisco activase: Rubisco's catalytic chaperone. Photosynth Res **75:** 11–27

Portis AR Jr, Li C, Wang D, Salvucci ME (2008) Regulation of Rubisco activase and its interaction with Rubisco. J Exp Bot **59:** 1597–1604

Ristic Z, Momčilović I, Bukovnik U, Prasad PVV, Fu J, Deridder BP, Elthon TE, Mladenov N (2009) Rubisco activase and wheat productivity under heat-stress conditions. J Exp Bot **60:** 4003–4014

Saeed I, Bachir DG, Chen L, Hu YG (2016) The expression of tarca2-α gene associated with net photosynthesis rate, biomass and grain yield in bread wheat (*Triticum aestivum* L.) under field conditions. PLoS ONE **11:** e0161308

Sage RF, Way DA, Kubien DS (2008) Rubisco, Rubisco activase, and global climate change. J Exp Bot **59:** 1581–1595

Salvucci ME, Crafts-Brandner SJ (2004) Relationship between the heat tolerance of photosynthesis and the thermal stability of Rubisco activase in plants from contrasting thermal environments. Plant Physiol **134:** 1460–1470

Salvucci ME, Osteryoung KW, Crafts-Brandner SJ, Vierling E (2001) Exceptional sensitivity of Rubisco activase to thermal denaturation in vitro and in vivo. Plant Physiol **127:** 1053–1064

Sánchez de Jiménez E, Medrano L, Martínez-Barajas E (1995) Rubisco activase, a possible new member of the molecular chaperone family. Biochemistry **34:** 2826–2831

Scafaro AP, Gallé A, Van Rie J, Carmo-Silva E, Salvucci ME, Atwell BJ (2016) Heat tolerance in a wild *Oryza* species is attributed to maintenance of Rubisco activation by a thermally stable Rubisco activase ortholog. New Phytol **211:** 899–911

Scales JC, Parry MA, Salvucci ME (2014) A non-radioactive method for measuring Rubisco activase activity in the presence of variable ATP: ADP ratios, including modifications for measuring the activity and activation state of Rubisco. Photosynth Res **119:** 355–365

Shivhare D, Mueller-Cajar O (2017) In vitro characterization of thermostable CAM Rubisco activase reveals a Rubisco interacting surface loop. Plant Physiol **174:** 1505–1516

Silva-Pérez V, Furbank RT, Condon AG, Evans JR (2017) Biochemical model of C_3 photosynthesis applied to wheat at different temperatures. Plant Cell Environ **40:** 1552–1564

Stotz M, Mueller-Cajar O, Ciniawsky S, Wendler P, Hartl FU, Bracher A, Hayer-Hartl M (2011) Structure of green-type Rubisco activase from tobacco. Nat Struct Mol Biol **18:** 1366–1370

To KY, Suen DF, Chen SCG (1999) Molecular characterization of ribulose-1,5-bisphosphate carboxylase/oxygenase activase in rice leaves. Planta **209:** 66–76

Wang Q, Serban AJ, Wachter RM, Moerner WE (2018) Single-molecule diffusometry reveals the nucleotide-dependent oligomerization pathways of *Nicotiana tabacum* Rubisco activase. J Chem Phys **148:** 123319

Wang ZY, Ramage RT, Portis AR Jr (1993) Mg^{2+} and ATP or adenosine 5′-[γ-thio]-triphosphate (ATPγS) enhances intrinsic fluorescence and induces aggregation which increases the activity of spinach Rubisco activase. Biochim Biophys Acta **1202:** 47–55

Yamasaki T, Yamakawa T, Yamane Y, Koike H, Satoh K, Katoh S (2002) Temperature acclimation of photosynthesis and related changes in photosystem II electron transport in winter wheat. Plant Physiol **128:** 1087–1097